Proceedings of 30th International Conference on Ocean, Offshore and Arctic Engineering
OMAE 2011
June 19-24, 2011, Rotterdam, The Netherlands

OMAE2011-49212

EXPERIMENTAL WAVE GENERATION AND CANCELLATION WITH A CYCLOIDAL WAVE ENERGY CONVERTER

Stefan G. Siegel*

Department of Aeronautics
United States Air Force Academy
Air Force Academy, Colorado, 80840
USA
Email: stefan@siegels.us

Marcus Römer

Department of Aeronautics
United States Air Force Academy
Air Force Academy, Colorado, 80840,
USA

John Imamura

Department of Aeronautics
United States Air Force Academy
Air Force Academy, Colorado, 80840,
USA

Casey Fagley

Department of Aeronautics
United States Air Force Academy
Air Force Academy, Colorado, 80840,
USA

Thomas McLaughlin

Department of Aeronautics
United States Air Force Academy
Air Force Academy, Colorado, 80840,
USA

ABSTRACT

We investigate a lift based wave energy converter (WEC), namely, a cycloidal turbine, as a wave termination device. A cycloidal turbine employs the same geometry as the well established Cycloidal or Voith-Schneider Propeller. The main shaft is aligned parallel to the wave crests and fully submerged at a fixed depth. We show that the geometry of the Cycloidal WEC is suitable for single sided wave generation as well as wave termination of straight crested waves using feedback control.The cycloidal WEC consists of a shaft and one or more hydrofoils that are attached eccentrically to the main shaft. An experimental investigation into the wave generation capabilities of the WEC are presented in this paper, along with initial wave cancellation results for deep water waves. The experiments are conducted in a small 2D wave flume equipped with a flap type wave maker as well as a 1:4 sloped beach. The operation of the Cycloidal WEC both as a wave generator as well as a wave energy converter interacting with a linear Airy wave is demonstrated. The influence that design parameters radius and submergence depth on the performance of the WEC have is shown. For wave cancellation, the incoming wave is reduced in amplitude by $\approx 80\%$ *in these experiments. In this case wave termination efficiencies of up to 95% of the incoming wave energy with neglegible harmonic waves generated are achieved by synchronizing the rotational rate and phase of the Cycloidal WEC to the incoming wave.*

NOMENCLATURE

T Wave Period [s]
D Water Depth [m]
H Wave Height [m]
W Wave, index indicates type of wave
C Wave Travel Velocity (Celerity) [m/s]
C_g Wave Group Velocity [m/s]

*Address all correspondence to this author.

L Hydrofoil Lift Force [N]
c_L Lift Coefficient $c_L = \frac{L}{1/2\rho U_{\inf}^2 sc}$
C_r Beach Reflection Coefficient $C_r = \frac{H_{reflected}}{H_{incoming}}$
$U_{\inf}$ Freestream Velocity [m/s]
ρ Fluid Density $[kg/m^3]$
k Wave Number [1/m]
g Gravity constant, $9.81[m/s^2]$
t Time [s]
λ Wavelength [m]
$R = 60mm$ Wave Energy Converter Radius [m]
$c = 50mm$ Hydrofoil Chord [m]
$s = 550mm$ Hydrofoil Span [m]
x_c, y_c Wave Energy Converter Shaft location [m]
η Water Surface [m]
α Hydrofoil pitch angle relative to tangential direction [$\circ$]
γ Flap wave maker angle [$^\circ$]
T_F Wave maker period [s]
$\delta(t)$ Main Shaft rotational angle [$^\circ$]
θ Phase [$^\circ$] between wave maker and WEC main shaft

INTRODUCTION

Among alternative energy sources, wave power is one of the most abundant sources on earth. The World Energy Council according to [1] has estimated the world wide annual amount of wave power energy at 17.5 PWh (Peta Watt hours = $10^{12} kWh$). This amount of power is actually comparable to the annual world wide electric energy consumption, which is currently estimated at 16 PWh. Thus, wave power has the potential to provide a large portion of the worlds electric energy needs, if it can be harnessed efficiently. In addition to the energy availability, wave power has other advantages. Since a large portion of the worlds population lives close to the ocean shores, the distance between energy production and consumption is small which reduces transmission losses and necessary investments in transmission lines. As opposed to other alternative energy sources like wind, stream and solar energy, the installation of wave power devices does not require use of already precious real estate. This makes wave power an ideal energy source for efficiently providing renewable energy to densely populated coastal areas. Ocean waves have a tremendous potential to provide clean renewable energy. Further engineering aspects of wave power as an energy source are appealing as well. While the power density of both solar and wind in typical favorable sites is in the order of $1 kW m^{-2}$ [2], wave power in a typical North Atlantic wave that was considered in a related paper [3] (wave height of $H = 3.5m$ and period of $T = 9s$) yields $108 kW m^{-1}$ of wave crest. As shown there, a device extending about $40m$ in the vertical direction can extract almost all of this wave power, yielding a power density of about $2.7 kW m^{-2}$ or more than twice that of wind or solar power. If one considers the theoretical inviscid conversion limits for waves and wind, which are 100% for waves [4] and 59% for wind [5], the accessible power density of waves is more than four times as large as that of wind. Furthermore, wave energy is available on a more consistent basis and can be better predicted in advance, therefore mitigating the need to back up a wave power plant with other conventional power sources, as is the case for both solar and wind energy.

MOTIVATION

Analysis of the different wave energy conversion devices that have been investigated or proposed reveals a number of commonalities in design. The first is that all devices require a connection to the sea bed in order to extract energy, which has two main drawbacks. First, a seabed connection makes the device vulnerable in rough seas and storms, in the same way as an anchored ship is vulnerable in a storm (and will likely break the anchor line). According to [1], storm survivability has been a major problem for many wave energy converters, with some being destroyed by the elements as early as during deployment. Also, for most of the devices, the load imposed onto the seabed connection is proportional to the power which the device can extract. This means that the anchor point needs to be stronger and thus more costly as more energy is being extracted. Therefore, many of these devices cannot easily be scaled up to power plant levels of energy conversion. In addition, since the devices need to be anchored to the sea floor, they are not well suited to operation in deep water waves, where the ocean floor may be hundreds of meters away from the surface. However, most wave energy is contained in deep water waves, and the energy density of a wave decreases as it approaches shallow water. Thus, most devices cannot operate in the most promising locations for wave power extraction.

Beyond survivability, efficiency has been a major issue for many WEC designs. While wave energy as a resource may be for free, the construction effort to harness it is a major expense and to a large degree determines the cost of energy being produced. As a less efficient WEC will need to be larger in size to extract the same amount of energy as a more efficient one, cost of energy is directly related to efficiency. Arguably, the most efficient WEC is one that can extract all of the energy from an incoming wave, and the class of wave energy converters that is able to achieve this is commonly referred to in literature as wave termination device. There have been various wave termination designs reported in literature, with the most well known devices being the Salter Duck [6] and the Bristol or Evans Cylinder [7]. Both consist of a series of elements which are aligned parallel to the wave crests, in the case of the Salter Duck these are cam shaped and floating on the surface, while the Bristol Cylinder is fully submerged. Both have been shown to be able to absorb an incoming wave completely. The wave energy is converted to electric power by means of a power take off system that is hydraulic in both cases. As both devices move at approximately the wave induced water

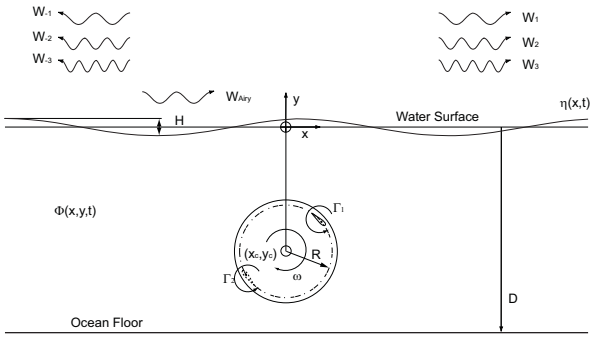

Figure 1. Cycloidal wave energy converter geometry and generated waves

velocity, the devices need to feature a large surface area to convert appreciable amounts of power. This increases construction cost, reduces storm survival odds and has ultimately motivated the investigation of the Cycloidal WEC described here. The fact that both devices require mooring to the ocean floor also hampers storm survival odds and precludes installation in very deep water.

A typical cycloidal wave energy converter (CycWEC) as considered in this paper is shown in figure 1. It features one or more hydrofoils attached eccentrically to a main shaft at a radius *R*. While the shaft rotates, the pitch angle of the blades may be adjusted. This device operates at a rotational speed of the hydrofoil that is typically an order of magnitude larger than the wave induced water velocity, and employs the lift force at the hydrofoil to generate shaft torque directly. Using lift allows for a much smaller hydrofoil planform area to be employed compared to the cross sectional areas of Duck and Cylinder, and generating shaft torque directly eliminates the need for a costly and inefficient hydraulic power take off system. In addition, it is conceptually possible to join several CycWECs into a cluster where the reactive forces at the shaft can be made to cancel, which reduces or negates entirely the need for mooring and thus enables deep water deployment while improving storm survival odds (see Siegel [8] for sketches). A single rotating hydrofoil has first been investigated by Hermans et al. [9] both numerically and experimentally. While Hermans et al. reported very low wave energy conversion efficiencies (on the order of a few percent), Siegel et al. [3] were able to show in simulations that with improved sizing of the WEC as well as by using feedback control to synchronize the rotation of the foil with the incoming wave, wave termination with better than 99% inviscid efficiency is possible.

These successful wave termination simulation results provided the motivation to set up the small 1:300 scale experiment that we report on in this publication. The goal was to experimentally demonstrate wave termination in an experiment using a CycWEC, which had not been achieved to date. While the small scale precludes accurate direct shaft power measurments which are scheduled later this year at 1:10 scale, it does allow accurate measurement of the waves generated and terminated by the WEC. Thus, main numerical findings like single sided wave generation as well as device radius and hydrofoil size can be experimentally confirmed, which allows construction of a larger scale model with confidence. In addition, the small scale experiment serves as an important test bed for wave estimation and feedback control algorithm development and validation.

EXPERIMENTAL SETUP

The tunnel used for testing the cycloidal WEC was a 2D wave tunnel designed to provide a 1:300 scale model of a deep ocean wave. The full scale deep ocean wave, which was investigated numerically in [3] had a period of 9s, a wave length of 126.5m and at a wave height of 3.5m it carried about 105kW of power per meter of wave crest. It is represented in the present setup by a wave with a period of 0.5s and wave length of 0.39m; at a typical wave height of 20mm the scaled wave carries approximately 192mW of wave power per meter. The experiment consists of four subparts: Wave tunnel, Cycloidal Wave Energy Converter (CycWEC), Wavegauges and Data Acquisition (DAQ) and processing system. These are described in detail in the following subsections. There were two experimental objectives: First, to produce single sided waves with the CycWEC and to measure the wave height of the main wave as well as any parasitic harmonic waves. Second, produce waves with the flap maker and cancel them using the CycWEC as a wave termination device.

Wave Tunnel

The wave tunnel is shown as conceptual sketch in figure 2. It allows for the generation of waves with a period between 0.2 and 1.15 seconds, and consists of the following three parts:

i. The wave tank. The tank has an overall length of 5m, where 4.50 meter are usable for wave experiments between the flap wave maker and the beach, a width of 0.55m and a design water depth of 0.3m. The width of the tunnel is increased by 50mm on each side in the center test section, which allows the drive system of the CycWEC to be placed outside of the wave testing area by means of false walls. The eigenfrequency of the wave tunnel had a period of 5.5-6 seconds, which was determined by exciting the tunnel resonance using a step input at the wave maker.

ii. The beach. The beach, located at the right end of the tunnel, is a linear beach with a 1:4 slope. The main purpose is to prevent reflection of waves travelling left to right. In order to evaluate the wave reflections from the beach, the reflection coefficient was measured experimentally and also compared to predictions based on a well established numcerical model. At the design wave of $T = 0.5s, H = 20mm$ the reflection coefficient was measured by traversing two wave gauges using the ap-

proach described in [7] and found to be $C_r = 0.106$. This is less than the estimate from the numerical model described in [10], which for the design wave estimates the reflection coefficient to be $C_r = 0.17$. We thus consider the numerical model a worst case estimate, and given textbook statements that consider it difficult to achieve less than $C_r = 0.1$ [11] the beach was found to perform sufficiently well for the measurements at hand. No wave reflection prevention (e.g. wave cancelling wave maker) is available at the left end of the tunnel for waves traveling right to left, where the flap wave maker is located. This does not cause any significant impact on the results, though, since the wave heights on the up–wave side of the WEC model are minimal for all data presented.

iii. The flap wave maker. The flap wave maker is a plain flap hinged at the bottom of the tunnel. It is driven by a brush type servo motor driving two sprockets attached to a shaft spanning the tunnel, which engage in two arc gear segments located at both sides of the tunnel attached to the top of the flap. This setup provides gearing to match the torque characteristics of the servo motor to the torque requirements of the wave maker. It also ensures pure rotational motion of the flap without torsion. The servo motor is connected to a motion controller operating in position mode allowing for arbitrary motion wave forms with an update rate of 10ms. In the present investigations, a sinusoidal motion

$$\gamma(t) = A_F \sin(2\pi t/T_F) \tag{1}$$

was prescribed using a deterministic hardware timed LabVIEW loop. This setup has the advantage that both wave height and period can be computer controlled without any hardware adjustments. It does not provide any incoming wave cancellation since no force feedback is available. Given the resolution of 2000 pulses per revolution of the servo motor shaft mounted encoder, and the gear ratio of 10:1 an angular resolution of 0.018 degrees is achieved.

Figure 2 shows a sketch of the overall test setup. The flap wave maker generated waves at the left side of the tunnel, which travelled past the first wave gauge (up–wave wave gauge). In the center of the test section the wave reached the CycWEC. The resulting waves were measured by the second wave gauge, which is located at an equal distance from the CycWEC. After a short distance the waves dissipate their energy at the beach.

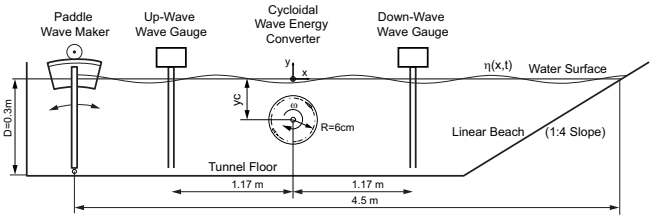

Figure 2. Wave tunnel schematic - not to scale

Wave Energy Converter Model

Based on the sketch in figure 1, a number of non dimensional quantities emerge. The basic size of the wave energy converter is denoted by $2R/\lambda$, where the wave length λ is the fundamental length scale. Consequently, the vertical position of the main shaft is denoted by y_c, and the wave height by H. It is also convenient for parameter studies to compare different size wave energy converters while keeping the distance between the water surface and the topmost point of the cycloidal wave energy converter path fixed, that is $|y_c| - R = const$. The direction of travel of an incoming ocean wave W_{Airy} is assumed to be left to right.Waves generated by the cycloidal wave energy converter that travel in the direction of the incoming wave receive a positive index and are considered traveling down–wave; while waves in the opposite direction are considered up–wave traveling and receive a negative index number.

The CycWEC device was designed to convert energy from waves to shaft power by wave cancellation. Figure 3 shows a picture, while the definition of the main geometry parameters is shown in figure 1. The only component interaction with the flow is a single hydrofoil spanning the tunnel. This hydrofoil is attached eccentrically at a radius $R = 60mm$, and has a NACA 4 series hydrofoil of $c = 50mm$ chord length with a camber line curvature to match the radius of the circle on which it rotates. The hydrofoil has a resulting camber line displacement of 11 percent, and the maximum thickness of 15% is located at 50% chord. This setup provides a zero lift pitch angle of $\approx 0^\circ$ and is expected to behave like the familiar NACA 0015 in straight flow, when rotating around a shaft. The pitch angle had to be adjusted manually and remained constant after it was set. The sign convention for the pitch angle is such that a rotation of the blade's leading edge towards the rotation center is negative, a rotation outward is positive. Setting the pitch angle manually only achieves a limited pitch angle accuracy, which we estimate to be about $\pm 0.5^\circ$.

The CycWEC is installed in the center of the wave tunnel such that the waves traveling the length of the tunnel are unobstructed but for the interaction with the CycWEC blade(s). The CycWEC can be operated with one or two blades, however all results presented in this paper were obtained with a single blade. The main shaft motor is located outside the water well above the tunnel, and connected directly to two timing belt sprockets. The timing belts engage in individual larger sprockets below the water line with a 5:1 gear ratio, which in turn hold the blades. The main shaft motor (Pittman model 4442 S012) is a brushless servo motor with a 500 lines/rev incremental encoder driving the main shaft directly, and connected to a closed loop servo motor controller (Copley Motion Accelnet ACJ-090-12) allowing the

Figure 3. Picture of wave energy converter with a single blade installed.

motor to operate both as motor or generator depending on the torque applied to the shaft. Together with the 5:1 gear ratio as well as edge detection of the encoder signals an overall resolution of 10000 counts/revolution is achieved. The motor controller was operated in position mode, with position updates transmitted every 10ms to the controller over the CAN bus system (see below). For the wave cancellation experiments, the main shaft motor updates were transmitted in sync with the flap wave maker position updates.

The depth to which the rotational center of the WEC is submerged below the mean water surface, y_c, can be adjusted from the surface to $y_c = -0.1m$. This is achieved by adjusting the supports on both sides of the WEC model, and is estimated to be accurate to $\pm 0.5mm$.

Wave Gauges

Two wire type wave gauges for wave height measurements were placed at a distance of $1.17m$ up– and down–stream of the WEC main shaft. The measurement of water level was by electrical resistance measurement. The wave gauges were operated with 2.5 V, 5khz AC and consisted of two stainless steel wires and a ground electrode. The signal from the wave gauges was first filtered by a high-pass analog filter to remove any DC offset, then rectified and again low-pass filtered with a corner frequency of 200Hz before it was amplified and digitized by a 10 bit A/D converter. The resulting measurements were transmitted over the same CAN bus system that the main shaft controller employed, using CANOpen as the data protocol. The wave gauges were calibrated for a measurement range of $y_m = 50mm$ before each measurement session, and the calibration was repeated after the last measurement run to verify that no drift in calibration had occured. The overall accuracy and repeatablitiy of the wave gage measurements is estimated to be better than $\pm 0.1mm$ based on the repeat calibration results, or $\pm 0.5\%$ of the design wave height.

DAQ and Post Processing

The entire experiment was controlled by a WINDOWS XP PC, using software written in LABView to transmit data over the CAN bus (Controller Area Network) to operate the wave maker, the wave gauges and the CycWEC. The received data was stored in Matlab files for post-processing. The sample rate of the system was 100 Hz for both position control as well as data acquisition, where all transmitted messages where synchronized using the CANOpen sync messages. Every measurement lasted 61 seconds, but only the last 50 seconds when the flow had reached a periodic state were used for data analysis.

RESULTS

In terms of waves in the far field, an optimal wave energy converter would create an out of phase wave with the same amplitude and wave length as the incoming wave, travelling in only one direction and exactly 180° out of phase with the incoming wave. This wave energy converter, commonly referred to in literature as a wave termination device, could extract 100% of the energy of the incoming wave in the theoretical inviscid limit. Of all wave energy converters currently proposed or investigated in open literature, no design can achieve this. One main reason lies in the difficulty of preventing the wave energy converter from producing waves in the up–wave direction. Any wave travelling in the up–wave direction will reduce the efficiency of the converter, even in the inviscid limit. The same holds true for harmonic waves traveling in any direction. For this reason, it is convenient to analyze the performance of a proposed wave energy converter in its ability to be a wave generator, before analyzing the interaction between the wave energy converter and an incoming wave. Thus the next section covers wave generation by the CycWEC, followed by wave cancellation results in the following section.

Wave Generation

Shown in figure 4 is a snapshot of the typical resulting surface wave pattern. The rotational period of the WEC is $T = 0.55s$, and its submergence depth $|y_c| - R = 15mm$. It can be seen that the dominant wave amplitudes occur on the down–wave side of the converter (foreground of the picture), while the up–wave surface elevations towards the flap wave maker are small. It can also be observed that there are small transverse waves present

Figure 4. Picture of water surface for wave generation using a single bladed wave energy converter. Wave Period $T = 0.55s$, blade pitch $\alpha = -7.5^\circ$, submergence $|y_c| - R = 15mm$.

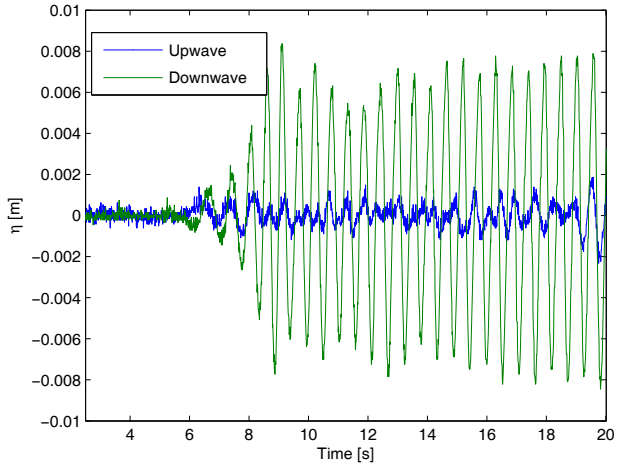

Figure 5. Surface Elevation at the up–wave and down–wave wave gage. For experimental parameters see caption of figure 4

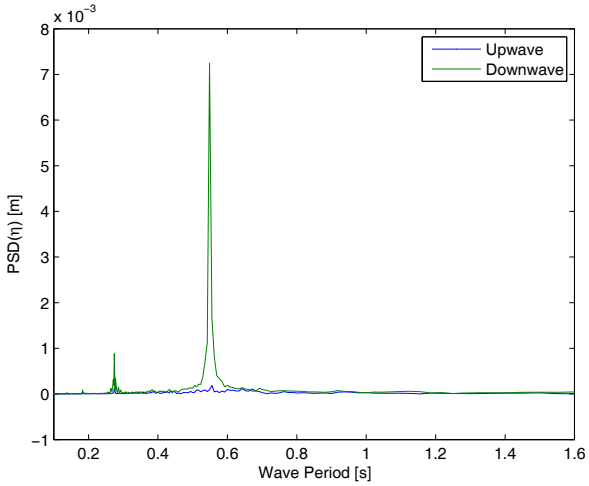

Figure 6. Power Spectral Density of the surface elevation at the up–wave and down–wave wave gage. For experimental parameters see caption of figure 4

in the tunnel which we found to be of small amplitude and thus negligible energy in all experiments conducted.

The corresponding wave gauge measurements are shown in figure 5. The measurements were started at $t = 0s$, while the CycWEC was started at $t = 5s$. After a short transient, both up– and down–wave wave gage readings indicate a periodic wave pattern with a small amplitude modulation, which is most likely caused by the tunnel eigenfrequency. It can also be observed that the wave traveling down–wave is much larger than the up–wave wave, while both feature the same dominant period which is identical to the rotational period of the WEC. For more detailed analysis, the periodic portion of the wave gage signals can be analyzed using a Fourier transform, the result of which is shown in figure 6. This analysis does not only yield quantitative amplitudes for the fundamental frequency, but also indicates the presence of a higher harmonic wave with half the wave period of the fundamental wave (i.e. $T = 0.275s$). This is again a typical result for all conducted measurements, where either the fundamental wave only, or a second harmonic wave in addition were found.

The wave amplitudes presented throughout this paper were determined based on the Fourier analysis results, where only data was used after the flow had reached a periodic state at both wave gauges. Thus, the wave heights reported in this paper represent the average wave height over the sampling period of 50s.

To determine the ability of the Cycloidal wave energy converter to produce waves of different wave length, a study was conducted where the WEC rotational period was varied. This effectively changes the ratio between WEC diameter 2R and the wave length λ. The experiments were conducted with constant pitch angle $\alpha = -5^\circ$ and constant submergence $|y_c| - R = 15mm$. Shown in figure 7 are wave amplitudes down–wave and up–wave for each of the first three harmonics. These were determined using power spectral density analysis as described above. The results are plotted as a function of $2R/\lambda_{Airy}$, where λ_{Airy} is the wave length of the fundamental wave. Inspecting the wave height of the fundamental wave traveling down–wave, H_1, a spread out maximum can be observed for values of $0.3 < 2R/\lambda_{Airy} < 0.7$. The wave height of the second harmonic wave reaches a maximum at smaller device sizes of $2R/\lambda_{Airy} = 0.15$. All other harmonic waves in this direction exhibit negligible amplitudes. No significant wave amplitudes were found for any fourth and higher harmonic waves for any of the experiments conducted, which is why they are not shown.

For a device size $2R/\lambda_{Airy} = 0.3$ the velocity ratio U_{rot}/C_{Airy} is close to unity indicating a match between hydrofoil rotation velocity and wave travel velocity. As $2R/\lambda_{Airy} = 0.32$ is the device size for which the fundamental wave height is maximized (see figure 7), it appears that the fundamental wave amplitude

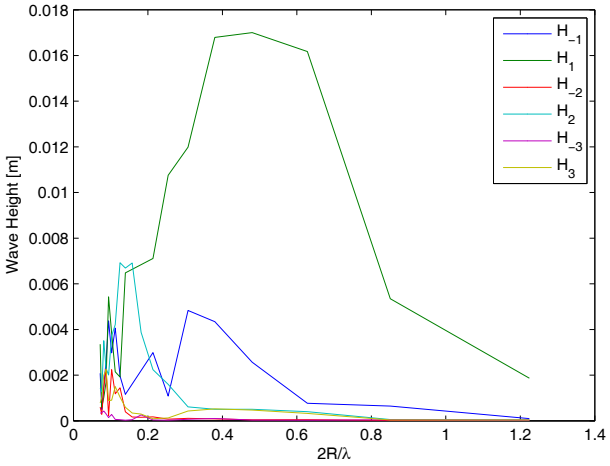

Figure 7. Wave height for different sizes $2R/\lambda$ of the cycloidal wave energy converter submerged to $|y_c| - R = 15mm$. Single blade WEC, blade pitch $\alpha = -7.5^\circ$

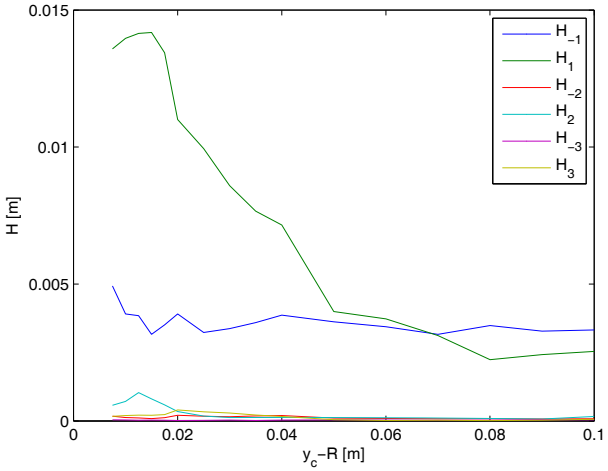

Figure 8. Generated wave heights as a function of submergence depth $|y_c| - R$ for a wave period of $T = 0.5s$. Single blade WEC, blade pitch $\alpha = -5^\circ$

is maximized if the velocity of the hydrofoil matches that of the wave. Further evidence that this is true can be gained by inspecting the harmonic wave amplitudes in figure 7. Not just is the amplitude of the fundamental wave height H_1 maximized at the same device size, but the peak amplitudes of the harmonic waves that travel at half (for W_2) and one third (for W_3) of the celerity of the fundamental wave occur at exactly one half or one third of the device size, which is $2R/\lambda_{Airy} = 0.15$ and $2R/\lambda_{Airy} = 0.1$ respectively. Thus, the generation of all harmonic waves is maximized once the hydrofoil travel velocity matches the respective wave celerity. Based on these observations we conclude that for optimal wave generation two design conditions have to be met:

$$\begin{aligned} \omega_c R &= C_{Airy} \\ \omega_c &= \omega_{Airy}. \end{aligned} \tag{2}$$

This result makes also physical sense as Airy wave theory assigns a distinct wave celerity to each wave of a given period, and thus waves with a mismatch between their period T and the celerity C induced by the vortex velocity can not be sustained.

Postulating a match of hydrofoil velocity and wave celerity as expressed in equation 2, we obtain with the airy wave equation the following optimal device size:

$$\frac{2R}{\lambda_{Airy}} = \frac{1}{\pi} \approx 0.318. \tag{3}$$

This result is independent of the type of wave, that is it holds for shallow, intermediate and deep water waves. In [3] numerical results show that the interaction of the cycloidal wave energy converter with deep ocean waves yields the exact same optimal device size, both for single vortex as well as flat panel simulations.

A second parameter study where the wave energy converter size was kept constant while the submergence depth y_c/λ was varied is shown in figure 8. We present the results of this study for a wave period $T = 0.5s$. Only three waves of significant height can be observed, H_1, H_{-1} and H_2. The fundamental wave H_1 is the dominant wave for all submergence heights down to $|y_c| - R = 60mm$, beyond which the fundamental up–wave wave H_{-1} becomes more dominant. The closer the WEC is placed relative to the surface, the larger the fundamental wave H_1 becomes reaching a maximum of about 14mm. Very close to the surface a decline in the fundamental wave amplitude can be observed when $|y_c| - R < 10mm$. This result indicates that there exists a optimal submergence depth for the WEC, which is for values of $10mm < |y_c| - R < 20mm$.

To determine the impact of the blade pitch angle on the waves generated, the blade pitch angle was varied from -35° to 15°. The results of these measurements are shown in figure 9. The submergence depth was kept constant at 12.5mm. While there is some variation for the different rotational periods shown, the created fundamental wave height reaches a minimum at a pitch angle of $\alpha = 0^\circ$ as expected. For all investigated rotational periods, the chord Reynolds number of the hydrofoil is well below $Re = 80k$, for which lift and drag coefficient data for a typical symmetric hydrofoil are shown in figure 10. The literature data shows an almost linear increase in lift up to a stall angle of $\alpha = \pm 10^\circ$. This correlates well with the wave generation

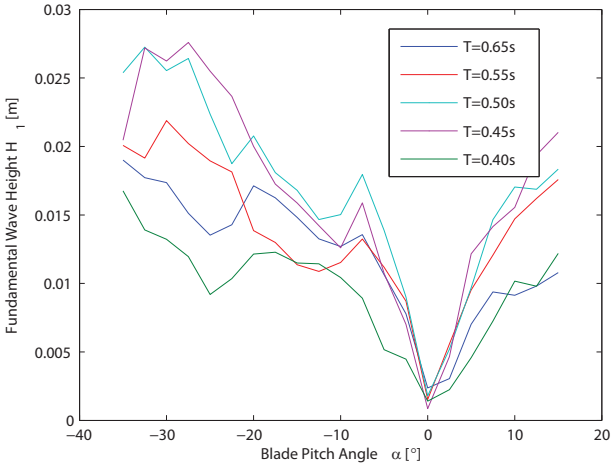

Figure 9. Generated fundamental wave height H_1 as a function of blade pitch angle. Submergence depth $y_c - R = 12.5mm$

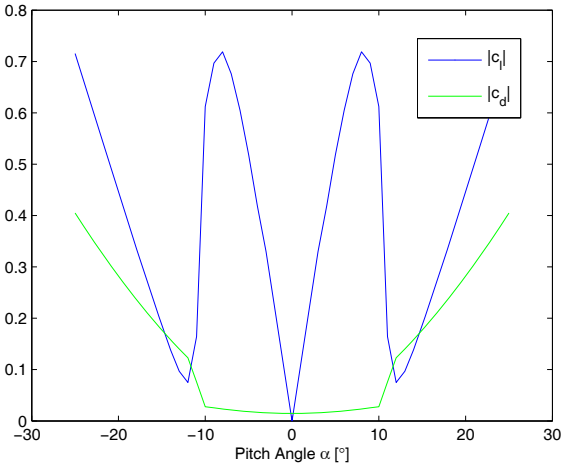

Figure 10. NACA 0015 Lift and drag coefficients from literature [12], $Re = 80 \times 10^3$

which shows a similar symmetric linear increase in wave height for up to 10 degrees in both directions. This linear correlation in generated wave height with the lift generated is in excellent agreement with the inviscid simulations reported in [3] where a linear dependence between vortex circulation and wave height was found. Also, no vortex circulation resulted in no waves being generated. This matches the zero wave height observed in figure 9 for zero angle of attack. Beyond stall, a further increase in lift can be observed in both figure 9 and figure 10 indicating that the correlation between circulation/lift and wave height holds even beyond stall in the experiment, where no simulation data is available for comparison. The literature data does show a more pronounced reduction in lift beyond stall, than the wave generation data does where only a slight reduction in generated wave height is observed beyond the stall angle of attack, before the generated wave heights increase again.

Wave Cancellation

With the CycWEC wave making performance characterized in the previous section, it is interesting to attempt cancellation of an incoming Airy wave. In order to synchronize the wave energy converter with an incoming wave, typically feedback of the incoming wave amplitude and phase to the motion of the cycloidal wave energy converter is employed. In the present experiment, we chose a simpler approach that can be implemented without the need for a real time controller or state estimator. As the waves are generated under computer control, their amplitude, frequency and phase are known a priori. At the same time, the wave height generated by the WEC for a certain wave period and blade pitch angle is known from the results presented in the previous section. Thus, it is possible to synchronize the flap wave maker and the CycWEC in the following fashion:

$$\begin{aligned} \delta(t) &= \omega_F\, t + \theta \\ \alpha &= -5^\circ \\ A_F &= 1^\circ. \end{aligned} \tag{4}$$

where $\delta(t)$ is the angle of the cycloidal wave energy converter main shaft, and θ is a constant phase shift between the wave motion prescribed for the paddle and the converter shaft rotational angle. The amplitudes of the flap wave maker and the blade pitch were chosen such that the amplitude of the wave H_1 created by the wave energy converter matches that of the wave generated by the wave maker on average. Figure 11 demonstrates the impact of the phase between the incoming wave and the rotation of the cycloidal propeller on the wave height. While there is very little impact of the feedback phase on all waves other than the fundamental wave down–wave as well as up–wave of the converter, the down–wave amplitude shows a steep increase for feedback phases above and below the optimal phase angle $\theta = -90^\circ$. The resulting down–wave wave pattern as a function of time is shown in figure 12 for the optimal feedback phase of $\theta = -90^\circ$. For this phase, the fundamental down-wave amplitude is reduced by about 80%. In this experiment, more than 95% of the incoming wave energy is extracted from the wave, with little energy lost to harmonic waves as seen in the wave height plot. The up–wave wave height is also affected by the phase of the feedback, where a reduction in up–wave wave height can be seen for phase angles of $\theta < -90^\circ$. This effect is most likely caused by refraction of the incoming wave at the wave energy converter blades. The same experiment is also shown in figure 14 where a snapshot of the water surface during wave cancellation can be seen. The incoming wave travels from the left front towards the

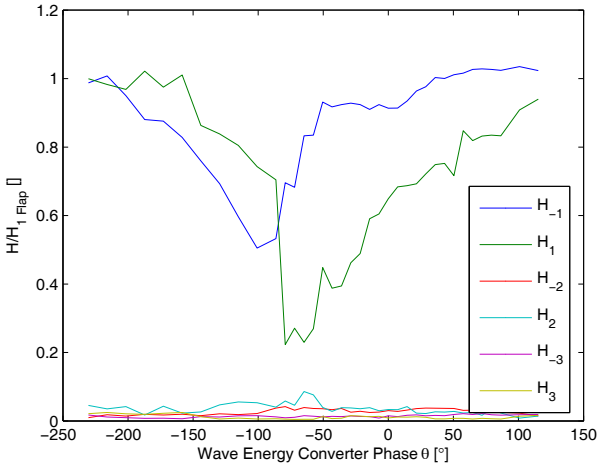

Figure 11. Fundamental wave heights as a function of feedback phase θ. Incoming wave period $T = 0.5s$, wave height $H = 17mm$, WEC has a single blade, blade pitch angle $\alpha = -5°$, submergence $|y_c| - R = 10mm$.

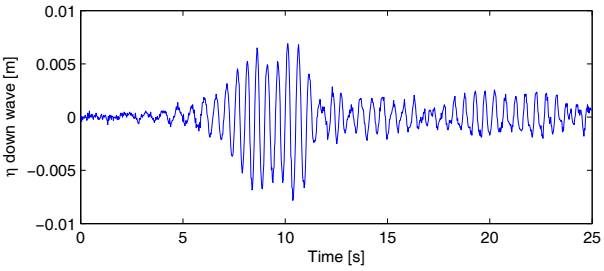

Figure 12. Down Wave water surface elevation during feedback controlled wave cancellation. Incoming wave period $T = 0.5s$, wave height $H = 13mm$, WEC has a single blade, feedback phase $\theta = -90°$, blade pitch angle $\alpha = -5°$, submergence $|y_c| - R = 10mm$.

right rear of the picture, and is cancelled at the WEC which is located just above the center of the picture. Down–wave from the WEC mostly short wave length harmonic waves can be observed. At the same time, no change in up–wave wave height can be observed as seen in the signal from the up–wave wave gage, figure 13.

DISCUSSION AND SUMMARY

The main result from this experimental study is the successful wave energy conversion of a harmonic, two dimensional deep ocean wave using a lift based, cycloidal wave energy converter. By synchronizing the wave energy converter to the incoming wave and matching the wave height, we achieve a 80% reduction in wave height and thus more than 95% energy conversion. Both harmonic waves and up–wave traveling waves are of neglegible

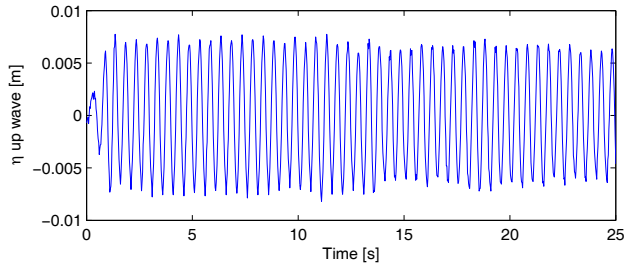

Figure 13. Up wave water surface during feedback controlled wave cancellation. For experimental parameters see caption figure 12

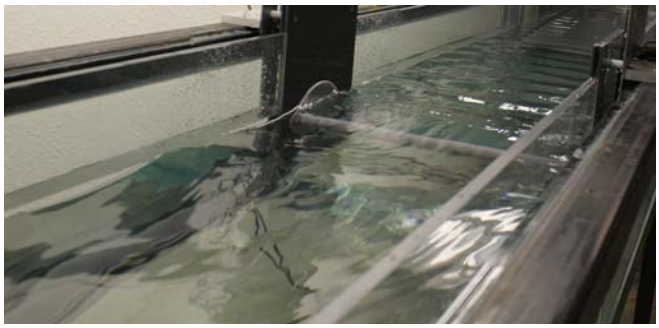

Figure 14. Picture of Water surface during feedback controlled wave cancellation at time $t = 18s$. For experimental parameters see caption figure 12

amplitude and energy. The wave energy converter of a given size is able to produce or cancel waves over a range of wave lengths spanning a factor of 5, or a factor of 2.2 in wave period. The optimal submergence is 2.5-5% of the incoming wave length below the surface, and the optimal size a diameter of $1/\pi$ or about 32% of the incoming wave length. For efficient wave cancellation accurate synchronization of the rotation of the wave energy converter to the phase of the incoming wave is shown to be crucial by means of a parameter study that reveals a large reduction in efficiency for small phase deviations.

Comparison to Simulation Results

All of the results in the previous section are in good agreement with potential flow simulations reported in [3]. In particular, the simulations found the same optimal device size of $2R/\lambda = 1/\pi$, and a range of efficient wave energy conversion for variations in wave length that also spans a factor of 5. The reduction in the simulation for feedback phase deviations was also very pronounced and linear in the close vicinity of the optimal phase. The simulations show a linear variation of the generated wave height with hydrofoil circulation, and the variation of the blade pitch shown in figure 9 also finds linear wave height increase with increasing hydrofoil pitch angle and thus circulation,

at least up to stall. The main differences between simulation and experimental results can be tracked to viscous effects at the hydrofoils - which were not modeled in the inviscid simulations. A main complication is the very low Reynolds number at the blades, which severely limits the ability of the hydrofoil to generate lift. While a typical hydrofoil at high Reynolds numbers will stall at pitch angles of about 15° or more, stall in this experiment occurred well below 10°. This limits the height of the waves that can be generated, where the simulations will show linear increase in wave height without any limits.

While the simulations results showed a reduction in wave amplitude of more than 99%, the experiment has not quite achieved this – yet. Part of the difference in cancellation efficiency can be attributed to the fact that we are only able to match the amplitude of incoming wave and wave maker generated wave in the present experiment on average. The actual wave amplitude however varies slowly in time, in part due to modulation with the tunnel eigenfrequency. As the actual measurement of the instantaneous incoming wave height was not used to adjust the blade pitch angle, it is not possible to achieve a perfect match between both wave heights. We expect this to improve as we implement computer controlled pitch control along with actual feedback in a future upgrade to this experiment.

It should be noted that the design objective of this experiment was to correctly scale the wave related parameters, such as the ratio between diameter of the WEC and incoming wave length. As a side effect, no match in blade Reynolds number could be achieved. Thus, the differences between simulation and experiment are inherent in the experimental setup.

Another notable difference between experiment and simulation was found when attempting two hydrofoil wave generation experiments. Based on the simulation results, we expected a fundamental wave of about twice the amplitude when adding a second hydrofoil of opposite pitch angle placed 180 degrees apart. However, the resulting waves were either equal or in some cases even reduced in amplitude. A working hypothesis for this behavior is that the wake shed by the first hydrofoil reduces the lift generated by the second hydrofoil. As the wake deficit is large compared to the hydrofoil size, based on boundary layer estimates about 15mm or more than 25% of the chord of the foil, the following foil experiences a drastically reduced flow velocity. This will reduce the lift, and consequently the generated wave heigth. In addition, since the distance and thus time for the wake to decay is reduced, the incoming flow velocity is even less than in the case of a single hydrofoil when the first hydrofoil passes the same location the second time.

Scaling to Larger Experiments and Full Ocean Size

As the CycWEC is scaled up to a larger scale experiment or full ocean prototype, it is expected that viscous problems described in the previous section will be reduced if not eliminated. This is due to the fact that the blade Reynolds number of $Re < 50 \times 10^3$ will increase to $Re > 10^6$ for a full scale prototype. In this case the inviscid assumption of the simulation applies more closely to the actual flow than in the present experiment. While the blade chord will increase in size for the full scale WEC, the ratio between boundary layer thickness and hydrofoil chord will be reduced from more than 25% in the present experiment to less than 0.2% for a full scale WEC. Thus, the wake will not dominate the inflow of a following hydrofoil. At the same time the time interval within which the wake from the first hydrofoil will arrive at the second hydrofoil will increase from about 180ms in the present experiment to more than 4s at full scale, or more than 20 fold. All of these effects will reduce the viscous effects that hamper the current experiment. Thus, we expect less viscous effects for the 1:10 scale experiments that are planned for the summer of 2011, and yet less viscous impacts for a full scale ocean prototype to be tested in the future. Sketches of a typical ocean implementation of this type of WEC can be found in [8].

ACKNOWLEDGMENT

We would like to acknowledge the support of Dipl. Ing. Sascha Koslek at TU Berlin in setting up the resistive wave gauges used in this experiment. We would also like to acknowledge fruitful discussion with Dr. Jürgen Seidel and Dr. Tiger Jeans. This material is based upon activities supported by the National Science Foundation under Agreement No. ECCS-0801614, monitored by Dr. George Maracas. Any opinions, findings, and conclusions or recommendations expressed are those of the authors and do not necessarily reflect the views of the National Science Foundation.

REFERENCES

[1] Boyle, G., 2004. *Renewable Energy - Power for a sustainable future*. Oxford University Press.

[2] Bedart, R., 2005. Final summary report - offshore wave power feasibility demonstration project. Tech. rep., E2I EPRI Global, WP 009 - US Rev 1.

[3] Siegel, S. G., Jeans, T., and McLaughlin, T., 2011. "Deep ocean wave energy conversion using a cycloidal turbine". *Applied Ocean Research,* ***accepted and in press***.

[4] Evans, D. V., 1976. "A theory for wave-power absorption by oscillating bodies". *J. Fluid Mech.,* ***77***(1), pp. 1–25.

[5] Betz, A., 1920. "Das maximum der theoretisch möglichen ausnützung des windes durch windmotoren". *Zeitschrift für das gesamte Turbinenwesen,* ***26***, pp. pp. 307–309.

[6] Salter, S. H., 1989. "World progress in wave energy-1988". *International journal of ambient energy,* ***10***(1), pp. 3–24.

[7] Evans, D. V., Jeffrey, D. C., Salter, S. H., and Taylor, J. R. M., 1979. "Submerged cylinder wave energy device:

theory and experiment". *Applied Ocean Research,* ***1***(1), pp. 3–12.

[8] Siegel, S. G., filed in 2006, awarded 2010. "Cyclical wave energy converter". *U. S. Patent 7,686,583 and pending / awarded International Patent applications*.

[9] Hermans, A. J., van Sabben, E., and Pinkster, J., 1990. "A device to extract energy from water waves". *Applied Ocean Research Computational Mechanics Publications,* ***Vol. 12, No. 4***, p. 5.

[10] Seelig, W., 1983. "Wave reflection from coastal structures". In Proceedings of Coastal Structures, American Society of Civil Engineers (ASCE), pp. 961–973.

[11] Cruz, J., 2008. *Ocean wave energy: current status and future prepectives*. Springer-Verlag.

[12] Sheldahl, R., and Klimas, P., 1981. Aerodynamic characteristics of seven symmetrical airfoil sections through 180-degree angle of attack for use in aerodynamic analysis of vertical axis wind turbines. Tech. Rep. SAND80-2114, Sandia National Laboratories.